Relevance of soil-pile tangential tractions for the estimation of kinematic seismic forces: Formulation and setting of a Winkler approach*

Guillermo M. Álamo*, Jacob D.R. Bordón, Juan J. Aznárez, Orlando Maeso

Insituto Universitario de Sistemas Inteligentes y Aplicaciones Numéricas en Ingeniería (SIANI),
Universidad de Las Palmas de Gran Canaria, Edificio Central del Parque Científico y Tecnológico,
Campus Universitario de Tafira 35017 Las Palmas de Gran Canaria, Spain
guillermo.alamo / jacobdavid.rodriguezbordon / juanjose.aznarez / orlando.maeso @ulpgc.es

Abstract

The effects of considering the tangential tractions that act on the soil-pile interface in the estimation of the pile seismic response are studied through a Beam on Dynamic Winkler Foundation model, which includes the distributed moments produced by the rotation of the pile cross-section and the action of the incident field. The performance of the developed Winkler formulation is evaluated by using a rigorous continuum model based on boundary elements that allows the use of both smooth and welded contact conditions at the soil-pile interface. In order to do the analyses, the seismic response of a fixed-head single pile embedded in different soils subjected to planar shear waves is computed in terms of envelopes of maximum bending moments and shear forces. Two soil profiles are assumed: homogeneous and two-strata halfspaces. The tangential tractions are found to significantly increase the pile maximum shear forces, but to have a minor impact on the pile maximum bending moments. The proposed Winkler model accurately reproduces the results of the continuum formulation for both contact conditions. However, some differences are found in the evaluation of the inter-layer envelopes, for which the simplified model underestimates their values.

Keywords: pile foundation, soil-structure interaction, kinematic interaction, BDWF model, boundary elements, tangential tractions

1 Introduction

The seismic response of pile foundations has been a demanding object of study in the soil-structure interaction field for the last decades. In the event of earthquake, seismic waves

*Pre-print of the paper published in APPLIED MATHEMATICAL MODELLING, 59, 1-19 (2018), DOI: 10.1016/j.apm.2018.01.025

will deform the pile originating internal forces along its length. Based on field evidences and experimental tests [1–4], it has been concluded that those kinematic forces can be as significant as the ones produced by the vibration of the supported structure (inertial forces) in the pile failure.

Among the different approaches that can be used for the analysis of the soil-pile system, the Beam on Dynamic Winkler Foundation (BDWF) model is a common choice. Although this kind of model was initially designed and still used for studying beams resting over the soil [e.g. 5–7], it also has a wide application in the modelling of embedded piles [e.g. 8–10]. Regarding the use of the BDWF model for computing the seismic response of pile foundations, and with no intention of presenting a full literature review, authors want to cite some of the pioneering works [11–13], as well as recent studies [14–17], which prove that this approach is still up-to-date. The main benefits of BDWF models are their simple formulation, low computational requirements and the possibility of inclusion of nonlinear behaviour of soil just by modifying the springs and dashpots coefficients. However, only the linear scenario will be considered in this study.

The interaction between soil and pile is often reduced to the lateral stiffness of the soil. Nevertheless, in addition to the lateral soil reactions, tangential tractions can also arise along the soil-pile interface depending on the terrain characteristics. Regarding the Winkler formulation, the additional loads that those tangential stresses produce into the pile can be represented as distributed moments [18]. This approach is followed in the present work, distinguishing and detailing the different components of the distributed moment: the one related to the pile flexural effects and the one related to the action of the incident field.

The study at hand aims to (1) verify the ability of the proposed BDWF model to reproduce the pile response by comparing its results with a rigorous continuous formulation based on the Boundary Elements Method (BEM) and (2) analyse how the consideration of the tangential tractions affects the seismic response of the pile in terms of envelopes of stress and moment resultants.

In order to fulfil these two objectives, the paper is structured as follow: in Section 2 the problem under study is defined. Then, Section 3 describes both the Winkler and the continuum models, giving special attention to the inclusion of the loads produced by the tangential tractions. Finally, the obtained results are discussed in Section 4 followed by the main conclusions in Section 5.

2 Problem Statement

The problem under study corresponds to a pile of length L and diameter d embedded in a (in general) multilayered halfspace, as sketched in Fig. 1. The dynamical behaviour of the pile is determined by the following properties: Young's modulus E, density ρ, Poisson's ratio ν, shear modulus G, area A, moment of inertia I and shear coefficient α (Timoshenko's beam theory). No damping is assumed for the pile.

On the other hand, each layer j of the halfspace is treated as a homogeneous, isotropic, linear, viscoelastic domain with the following properties: Young's modulus E_s^j, density ρ_s^j, Poisson's ratio ν_s^j, shear modulus G_s^j, shear wave propagation velocity c_s^j and hysteretic damping coefficient β_s^j. The portion of the pile length that crosses each soil layer is

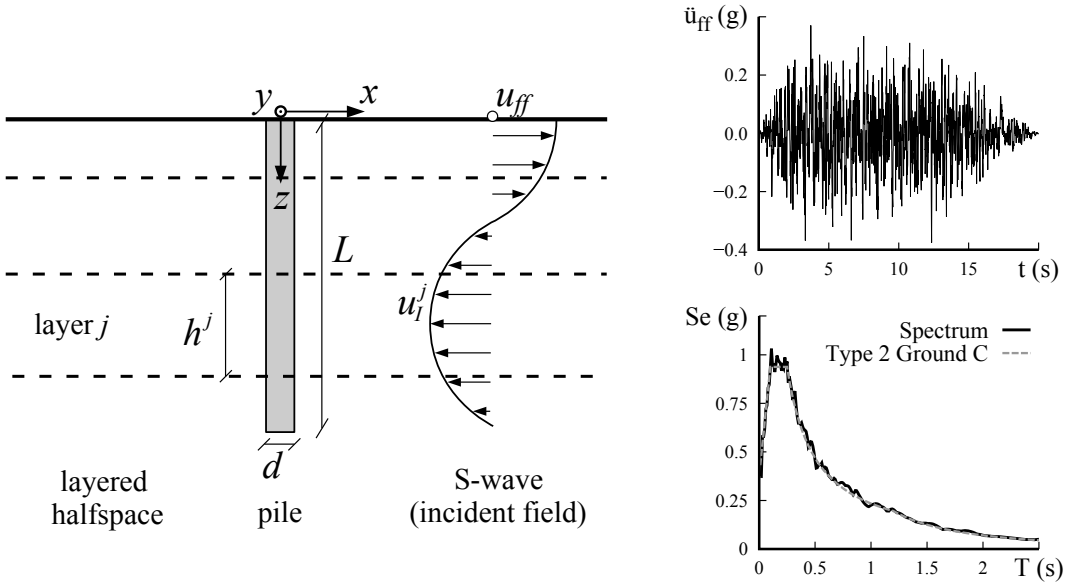

Figure 1: Problem under study. Artificial accelerogram and its spectrum used for the study

denoted as h^j.

The system is excited by planar shear waves that propagate vertically through the soil acting in the x direction. For each layer, the horizontal displacements that this incident field generates are obtained through the expression:

$$u_I^j(z) = A_I^j \mathrm{e}^{\mathrm{i}k_I^j z} + B_I^j \mathrm{e}^{-\mathrm{i}k_I^j z} \tag{1}$$

where A_I^j, B_I^j are the amplitudes of the incident and reflected waves for layer j obtained by solving the one dimensional wave propagation problem; $k_I^j = \omega/c_s^j$ is the wave number; i is the imaginary unit; ω is the angular frequency; and the term $\mathrm{e}^{\mathrm{i}\omega t}$ is omitted for simplicity's sake.

The problem is handled in the frequency-domain by both the BDWF and BEM methodologies. The transfer functions for the pile bending moments and shear forces with respect to the free field displacement u_{ff} are obtained and, then, their envelopes are calculated by computing the time response through the standard frequency-domain method [19]. For this purpose, one synthetic accelerogram compatible with the Type 2 response spectrum for Ground Type C [20] with a maximum acceleration equal to 0.375 g is used as excitation input (Fig. 1). This accelerogram is assumed to correspond to the free-field acceleration.

2.1 External loads due to the incident field

Attending to the expression of the incident field (Eq. 1), and omitting the soil layer super-index j for clarity's sake, the only term that does not vanish from the stress tensor σ_I is:

$$\tau_{xz_I}(z) = 2G_s\varepsilon_{xz_I} = G_s\frac{\mathrm{d}u_I}{\mathrm{d}z} \tag{2}$$

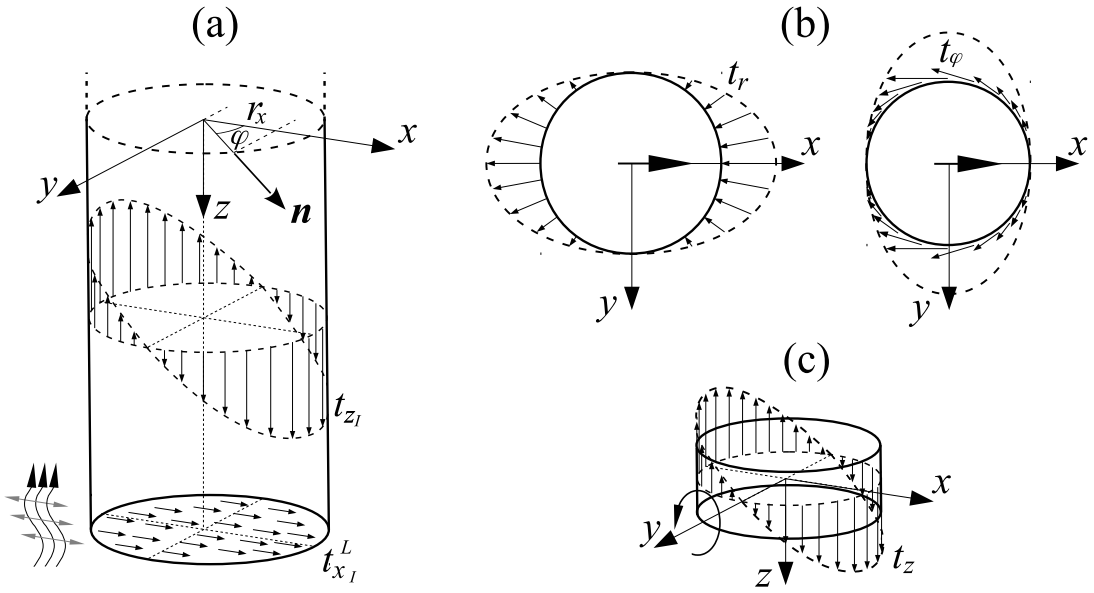

Figure 2: (a) Tangential tractions due to the incident field. (b) Normal and tangential tractions due to a horizontal displacement of the pile cross-section. (c) Tangential tractions due to a rotation of the pile cross-section

At a point of the soil-pile interface defined by the angle φ, see Fig. 2(a), with a normal vector $\mathbf{n} = (\cos\,\varphi, \sin\,\varphi, 0)$, the traction vector $\mathbf{t}_I$ is obtained as:

$$\mathbf{t}_I(z,\varphi) = \sigma_I \mathbf{n} = (0, 0, \tau_{xz_I}\,\cos\,\varphi) \tag{3}$$

This vertical tangential traction produces a moment m_y around the y axis equal to:

$$m_y(z,\varphi) = -r_x t_{z_I} = -r\tau_{xz_I}\cos^2\varphi \tag{4}$$

where r is the pile radius. Note that the moment is negative according to the sign criteria assumed.

The total distributed moment m_I acting over the pile cross-section can be finally obtained by integrating the punctual moment m_y over the soil-pile interface:

$$m_I(z) = \int_0^{2\pi} m_y r \mathrm{d}\varphi = -\pi r^2 \tau_{xz_I} = -\pi r^2 G_s \frac{\mathrm{d}u_I}{\mathrm{d}z} \tag{5}$$

By defining $K_I = \pi r^2 G_s$, one can express this distributed moment in a similar way than the Winkler's distributed soil reactions:

$$m_I(z) = -K_I \frac{\mathrm{d}u_I}{\mathrm{d}z} \tag{6}$$

On the other hand, considering the pile cross-section at tip level ($z = L$) with a normal defined by $\mathbf{n} = (0, 0, 1)$, the traction vector $\mathbf{t}_I^L$ is equal to:

$$\mathbf{t}_I^L = \sigma_I \mathbf{n} = (\tau^L_{xz_I}, 0, 0) \tag{7}$$

where super-index L indicates that the variable is evaluated at the end of the pile.

Integrating this horizontal component of the traction vector over the pile tip surface, the shear force produced at the end of the pile due to action of the incident field results in:

$$V_I^L = \iint_A t_{x_I}^L \mathrm{d}A = \pi r^2 \tau_{xz_I}^L = \pi r^2 G_s \frac{\mathrm{d}u_I}{\mathrm{d}z}\bigg|^L \tag{8}$$

3 Methodologies

3.1 Winkler model for an embedded Timoshenko's beam

In this section, the general differential equation that describes the dynamic lateral response of the pile subjected to lateral distributed forces and moments due to seismic excitation is written. The pile is modelled as a Timoshenko's beam and the different components of those loads are defined in order to include all phenomena that take place in the problem under study. The result of this procedure is a BDWF model that can be used to estimate the pile response (lateral displacements, rotations, shear forces and bending moments), which is sketched in Fig. 3(b).

The forces acting over a differential element of the beam are represented in Fig. 3(a). The translational and rotatory inertia of the beam are included in the terms q and m together with the distributed external forces and moments acting over it. Attending to this, the equilibrium equations of the beam differential element results in:

$$\frac{\mathrm{d}V}{\mathrm{d}z} + q = 0 \tag{9a}$$

$$\frac{\mathrm{d}M}{\mathrm{d}z} + V + m = 0 \tag{9b}$$

The Timoshenko's beam theory includes the effects of the warping of the beam cross-section produced by the shear stresses by assuming a constant value of the beam shear distortion γ_{xz}. The constitutive laws that determine the Timoshenko's beam bending

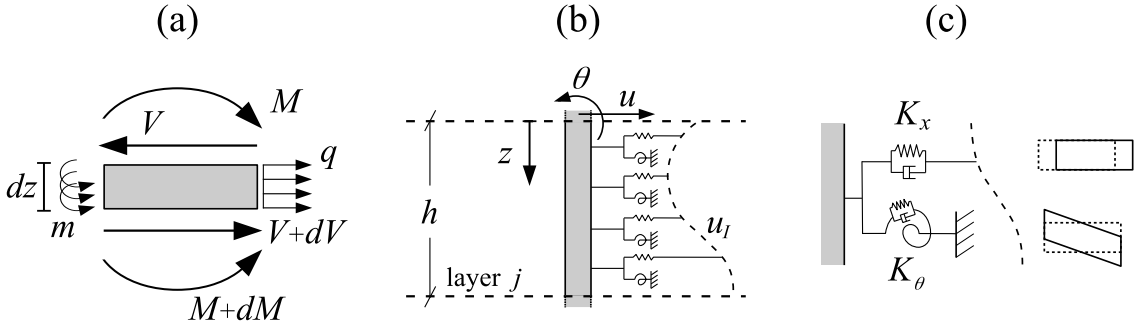

Figure 3: (a) Forces and moments acting over a differential element of the beam. (b) BDWF model for a pile embedded in a soil layer. (c) Winkler's soil impedance terms for different deformation modes

moment (M) and shear force (V) are:

$$M = EI\frac{\mathrm{d}\theta}{\mathrm{d}z} \tag{10a}$$

$$V = \alpha GA\gamma_{xz} = \alpha GA\left(\frac{\mathrm{d}u}{\mathrm{d}z} - \theta\right) \tag{10b}$$

where u is the lateral displacement of the beam and θ is the rotation of the beam cross-section produced only by the flexural effects.

Substituting the constitutive laws (10) in the equilibrium equations (9) and after some simple operations, the differential equation that governs the lateral displacements of the beam results in:

$$\frac{\mathrm{d}^4u}{\mathrm{d}z^4} + \frac{1}{\alpha GA}\frac{\mathrm{d}^2q}{\mathrm{d}z^2} - \frac{q}{EI} + \frac{1}{EI}\frac{\mathrm{d}m}{\mathrm{d}z} = 0 \tag{11}$$

While the beam rotation can be expressed in terms of the horizontal displacement as:

$$\theta = \frac{EI}{\alpha GA}\left[\frac{\mathrm{d}^3u}{\mathrm{d}z^3} + \frac{\alpha GA}{EI}\frac{\mathrm{d}u}{\mathrm{d}z} + \frac{1}{\alpha GA}\frac{\mathrm{d}q}{\mathrm{d}z} + \frac{1}{EI}m\right] \tag{12}$$

Considering now the different phenomena that participate in the studied problem, and omitting the soil layer super-index j for clarity's sake, the components of the distributed lateral force acting over the beam are:

$$q = \rho A\omega^2 u + K_x\left(u_I - u\right) \tag{13}$$

- $\rho A\omega^2 u$: distributed force due to the translational inertia of the beam.
- $K_x\left(u_I - u\right)$: distributed force produced by the soil lateral impedance K_x. This force is produced by the relative lateral displacement between the beam and the soil.

On the other hand, the different components of the distributed moment acting over the beam are:

$$m = \rho I\omega^2\theta - K_\theta\theta - K_I\frac{\mathrm{d}u_I}{\mathrm{d}z} \tag{14}$$

- $\rho I\omega^2\theta$: distributed moment due the rotational inertia of the beam cross-section.
- $-K_\theta\theta$: distributed moment associated with the soil rocking impedance K_θ. This moment is produced by the tangential tractions that arise in the soil-pile interface when the cross-section rotates.
- $m_I = -K_I\ \mathrm{d}u_I/\mathrm{d}z$: distributed moment produced by the tangential tractions that arise in the soil-pile interface due to the action of the incident field. The derivation of this component directly from the incident field equations and separately from the moment produced due to the reaction of the soil to the pile rotation constitutes a novel and theoretically more rigorous approach of this interaction effect in relation with similar previous models.

Table 1: Definition of the dimensionless parameters of the Winkler model

Definition	Expression
lateral stiffness-inertia ratio	$\kappa_1 = (h)^2 \left(K_x - \rho A \omega^2\right) / \alpha G A$
rotational stiffness-inertia ratio	$\kappa_2 = (h)^2 \left(K_\theta - \rho I \omega^2\right) / EI$
shear-flexural stiffness ratio	$\kappa_3 = (h)^2 \alpha G A / EI$
dimensionless lateral soil stiffness	$\kappa_4 = (h)^2 K_x / \alpha G A$
dimensionless incident field moment coef.	$\kappa_5 = (h)^2 K_I / EI$

Fig. 3(c) illustrates the different Winkler's soil impedances considered and the deformation modes associated with them. In this work, the expressions of the lateral and rocking soil impedances proposed by Novak et al. [21] are used. This set of soil impedances are chosen over other options [e.g. 13, 22–24] because they are obtained through an analytical procedure and have explicit expressions that do not depend on heuristic parameters.

Now, including the expressions of the distributed force (13) and moment (14) in Eqs. (11) and (12), after some algebraic operations (see A), and defining the set of dimensionless parameters shown in Table 1, the differential equation of the beam lateral displacement can be expressed in terms of the dimensionless axial coordinate $\xi = z^j / h^j$ as:

$$\frac{\mathrm{d}^4 u}{\mathrm{d}\xi^4} - (\kappa_1 + \kappa_2) \frac{\mathrm{d}^2 u}{\mathrm{d}\xi^2} + \kappa_1 (\kappa_2 + \kappa_3) u = \kappa_4 (\kappa_2 + \kappa_3) u_I - (\kappa_4 - \kappa_5) \frac{\mathrm{d}^2 u_I}{\mathrm{d}\xi^2} \tag{15}$$

By defining:

$$a_1 = \kappa_1 + \kappa_2 \tag{16a}$$
$$a_2 = \kappa_1(\kappa_2 + \kappa_3) \tag{16b}$$
$$a_3 = \kappa_4(\kappa_2 + \kappa_3) \tag{16c}$$
$$a_4 = \kappa_4 - \kappa_5 \tag{16d}$$

the solution that satisfies this differential equation can be obtained as the sum of the homogeneous and particular terms following the expression:

$$u(\xi) = C_1 \, \mathrm{e}^{\xi s_1} + C_2 \, \mathrm{e}^{\xi s_2} + C_3 \, \mathrm{e}^{\xi s_3} + C_4 \, \mathrm{e}^{\xi s_4} + C_P \, u_I(\xi) \tag{17}$$

where s_{1-4} are the roots of the homogeneous equation:

$$s_{1-4} = \pm \sqrt{\frac{a_1 \pm \sqrt{a_1^2 - 4a_2}}{2}} \tag{18}$$

C_P is the amplitude of the particular solution related to the dynamic loading (incident field):

$$C_P = \frac{a_3 + (k_I)^2 a_4}{(k_I)^4 + a_1 (k_I)^2 + a_2} \tag{19}$$

and C_{1-4} are the amplitudes of the homogeneous solution that are computed by imposing boundary conditions.

Once the pile lateral displacements are known, by including the expressions of the distributed loads (13), (14) into Eqs. (10) and (12) , the rotation of the cross-section, bending moment and shear force can be obtained as (see details in A):

$$\theta(\xi) = \frac{1/h}{\kappa_2 + \kappa_3} \left[\frac{\mathrm{d}^3 u}{\mathrm{d}\xi^3} - (\kappa_1 - \kappa_3) \frac{\mathrm{d}u}{\mathrm{d}\xi} + (\kappa_4 - \kappa_5) \frac{\mathrm{d}u_I}{\mathrm{d}\xi} \right] \tag{20}$$

$$M(\xi) = \frac{EI/(h)^2}{\kappa_2 + \kappa_3} \left[\frac{\mathrm{d}^4 u}{\mathrm{d}\xi^4} - (\kappa_1 - \kappa_3) \frac{\mathrm{d}^2 u}{\mathrm{d}\xi^2} + (\kappa_4 - \kappa_5) \frac{\mathrm{d}^2 u_I}{\mathrm{d}\xi^2} \right] \tag{21}$$

$$V(\xi) = \frac{-\alpha GA/h}{\kappa_2 + \kappa_3} \left[\frac{\mathrm{d}^3 u}{\mathrm{d}\xi^3} - (\kappa_1 + \kappa_2) \frac{\mathrm{d}u}{\mathrm{d}\xi} + (\kappa_4 - \kappa_5) \frac{\mathrm{d}u_I}{\mathrm{d}\xi} \right] \tag{22}$$

In this work, free displacement and fixed rotation conditions are assumed at pile head: $\theta(0) = 0$, $V(0) = 0$; while free tip conditions are considered at the end of the pile: $M(1) = 0$, $V(1) = 0$. In addition to the free tip conditions, the loaded tip assumption was also tested in the analyses yielding good results. For this loaded boundary condition, the shear force at the pile tip is imposed to be equal to the resultant of the horizontal tractions originated by the incident field at the pile end: $V(1) = V_I^L$, see Eq. (8) in Section 2.1.

For layered soil profiles, Eqs. from (15) to (22) are applied for each stratum and continuity boundary conditions for pile lateral displacements, rotations and resultants are also imposed at the depth of each layer interface:

$$u^j(1) = u^{j+1}(0) \tag{23a}$$

$$\theta^j(1) = \theta^{j+1}(0) \tag{23b}$$

$$M^j(1) = M^{j+1}(0) \tag{23c}$$

$$V^j(1) = V^{j+1}(0) \tag{23d}$$

It is important to notice that the obtained equations include all the phenomena that were described before. However, simpler formulations that neglect the contribution of some of the components can be directly obtained by nullifying the corresponding terms.

3.2 BEM model

A multi-region BEM approach is used to obtain a rigorous continuum mechanics solution of the problem. It uses the Singular Boundary Integral Equation (SBIE) for elastodynamics to build a solvable system of linear equations, from which unknown boundary displacements and tractions are obtained [25]. This model has been developed by the authors during the last years and it has been successfully used in a wide variety of dynamic problems. Several of the publications related contain verification results with solutions published by other authors [26], analytical solutions (the most recent [27]), and numerical results obtained by the authors themselves through other methodologies [28].

For computational reasons, it is crucial to exploit geometric and functional symmetry properties in this problem, see Fig. 4. They are enforced by using the element mirroring approach [29]. Planar shear waves are assumed to be acting in the x direction, hence $y - z$ plane is a plane of anti-symmetry, and $z - x$ plane is a plane of symmetry. Based

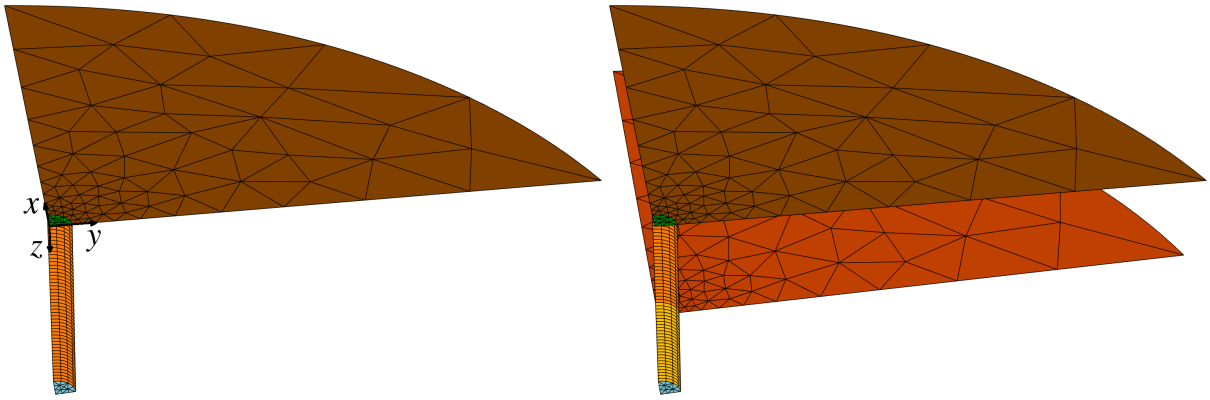

Figure 4: Multi-region BEM meshes. Left: homogeneous soil. Right: two-strata soil

on previous experience [see e.g. 25], meshes have been truncated at $3L$, and at least three quadratic elements per shear wavelength have been used. Nevertheless, a convergence test with respect to pile response has been performed, and it has been found that a finer mesh is needed for the pile and its surroundings.

The incident field is included in the BEM by posing the integral equations in terms of the scattered field for the soil region [25]:

$$\mathbf{H}\left(\mathbf{u}-\mathbf{u}_I\right)=\mathbf{G}\left(\mathbf{t}-\mathbf{t}_I\right) \tag{24}$$

where $\mathbf{H}$ and $\mathbf{G}$ are the influence matrices, $\mathbf{u}$ and $\mathbf{t}$ are displacements and tractions of the total field, and $\mathbf{u}_I$ and $\mathbf{t}_I$ are displacements and tractions of the incident field obtained from Eq. (1). The construction of these influence matrices follows well-known methodologies, [see e.g. 25]. The singularities present in integrals due to the fundamental solution (homogeneous full-space) are treated using the method of Li et al. [30] for weak singularities, and the method of line integrals of [31] for strong (Cauchy Principal Value) singularities. The free-term is analytically evaluated using the formulation of Mantič [32].

The final linear system of equations can be written as:

$$\mathbf{A}\mathbf{x}=\mathbf{b}+\mathbf{b}_I \tag{25}$$

where $\mathbf{A}$ and $\mathbf{b}$ are built from influence matrices and boundary conditions, and $\mathbf{b}_I = \mathbf{H}\mathbf{u}_I - \mathbf{G}\mathbf{t}_I$ is the load vector due to the incident field.

In the following, two particular features that have been developed for studying the problem at hand are described: the possibility of establishing a smooth contact condition between two regions, and a methodology for cross-section stress resultants calculation for the pile region.

3.2.1 Welded and smooth contact conditions

Let Ω_α and Ω_β be two regions in contact through an interface Γ_j. The interface Γ_j has two faces Γ_{j_+} and Γ_{j_-} whose orientations are compatible respectively with regions Ω_α and Ω_β. The boundaries of both regions are then $\partial\Omega_\alpha = \Gamma_{j_+} \cup \Gamma_i$ and $\partial\Omega_\beta = \Gamma_{j_-} \cup \Gamma_k$.

Displacements and tractions throughout $\partial\Omega_\alpha$ are related by the BEM influence matrices:

$$\begin{bmatrix} \mathbf{H}_{i,i} & \mathbf{H}_{i,j_+} \\ \mathbf{H}_{j_+,i} & \mathbf{H}_{j_+,j_+} \end{bmatrix} \begin{Bmatrix} \mathbf{u}_i \\ \mathbf{u}_{j_+} \end{Bmatrix} = \begin{bmatrix} \mathbf{G}_{i,i} & \mathbf{G}_{i,j_+} \\ \mathbf{G}_{j_+,i} & \mathbf{G}_{j_+,j_+} \end{bmatrix} \begin{Bmatrix} \mathbf{t}_i \\ \mathbf{t}_{j_+} \end{Bmatrix} \tag{26}$$

and analogously for $\partial\Omega_\beta$. Subscripts $\square_{l,m}$ for influence matrices denote collocation at boundary Γ_l and integration over boundary Γ_m.

For a welded contact condition: $\mathbf{u}_{j_+} = \mathbf{u}_{j_-}$ and $\mathbf{t}_{j_+} + \mathbf{t}_{j_-} = \mathbf{0}$; and the coupled system can be written as:

$$\begin{bmatrix} \mathbf{H}_{i,i} & \mathbf{H}_{i,j_+} & -\mathbf{G}_{i,j_+} & \varnothing \\ \mathbf{H}_{j_+,i} & \mathbf{H}_{j_+,j_+} & -\mathbf{G}_{j_+,j_+} & \varnothing \\ \varnothing & \mathbf{H}_{j_-,j_-} & \mathbf{G}_{j_-,j_-} & \mathbf{H}_{j_-,k} \\ \varnothing & \mathbf{H}_{k,j_-} & \mathbf{G}_{k,j_-} & \mathbf{H}_{k,k} \end{bmatrix} \begin{Bmatrix} \mathbf{u}_i \\ \mathbf{u}_{j_+} \\ \mathbf{t}_{j_+} \\ \mathbf{u}_k \end{Bmatrix} = \begin{bmatrix} \mathbf{G}_{i,i} & \varnothing \\ \mathbf{G}_{j_+,i} & \varnothing \\ \varnothing & \mathbf{G}_{j_-,k} \\ \varnothing & \mathbf{G}_{k,k} \end{bmatrix} \begin{Bmatrix} \mathbf{t}_i \\ \mathbf{t}_k \end{Bmatrix} \tag{27}$$

which must be understood as a part of the complete system if more regions or boundaries are present.

For a smooth contact condition, nodal displacements and tractions of the interface must be rotated into a local orthogonal system $(\mathbf{s}_1, \mathbf{s}_2, \mathbf{n})$ formed by a pair of orthonormal tangent vectors $\mathbf{s}_1$ and $\mathbf{s}_2$ and a normal vector $\mathbf{n}$. Once rotation is performed, the influence matrices for $\partial\Omega_\alpha$ can be expressed as:

$$\begin{bmatrix} \mathbf{H}_{i,i} & \mathbf{H}^s_{i,j_+} & \mathbf{H}^n_{i,j_+} \\ \mathbf{H}_{j_+,i} & \mathbf{H}^s_{j_+,j_+} & \mathbf{H}^n_{j_+,j_+} \end{bmatrix} \begin{Bmatrix} \mathbf{u}_i \\ \mathbf{u}^s_{j_+} \\ \mathbf{u}^n_{j_+} \end{Bmatrix} = \begin{bmatrix} \mathbf{G}_{i,i} & \mathbf{G}^s_{i,j_+} & \mathbf{G}^n_{i,j_+} \\ \mathbf{G}_{j_+,i} & \mathbf{G}^s_{j_+,j_+} & \mathbf{G}^n_{j_+,j_+} \end{bmatrix} \begin{Bmatrix} \mathbf{t}_i \\ \mathbf{t}^s_{j_+} \\ \mathbf{t}^n_{j_+} \end{Bmatrix} \tag{28}$$

where $\mathbf{u}^s_{j_+}$ and $\mathbf{t}^s_{j_+}$ gather tangent components, and $\mathbf{u}^n_{j_+}$ and $\mathbf{t}^n_{j_+}$ normal components. Influence matrices for $\partial\Omega_\beta$ can be written in a similar manner. Therefore, for a smooth contact condition: $\mathbf{u}^n_{j_+} = \mathbf{u}^n_{j_-}$, $\mathbf{t}^n_{j_+} + \mathbf{t}^n_{j_-} = \mathbf{0}$, $\mathbf{t}^s_{j_+} = \mathbf{t}^s_{j_-} = \mathbf{0}$; and the resulting coupled system is:

$$\begin{bmatrix} \mathbf{H}_{i,i} & \mathbf{H}^s_{i,j_+} & \mathbf{H}^n_{i,j_+} & \varnothing & -\mathbf{G}^n_{i,j_+} & \varnothing \\ \mathbf{H}_{j_+,i} & \mathbf{H}^s_{j_+,j_+} & \mathbf{H}^n_{j_+,j_+} & \varnothing & -\mathbf{G}^n_{j_+,j_+} & \varnothing \\ \varnothing & \varnothing & \mathbf{H}^n_{j_-,j_-} & \mathbf{H}^s_{j_-,j_-} & \mathbf{G}^n_{j_-,j_-} & \mathbf{H}_{j_-,k} \\ \varnothing & \varnothing & \mathbf{H}^n_{k,j_-} & \mathbf{H}^s_{k,j_-} & \mathbf{G}^n_{k,j_-} & \mathbf{H}_{k,k} \end{bmatrix} \begin{Bmatrix} \mathbf{u}_i \\ \mathbf{u}^s_{j_+} \\ \mathbf{u}^n_{j_+} \\ \mathbf{u}^s_{j_-} \\ \mathbf{t}^n_{j_+} \\ \mathbf{u}_k \end{Bmatrix} = \begin{bmatrix} \mathbf{G}_{i,i} & \varnothing \\ \mathbf{G}_{j_+,i} & \varnothing \\ \varnothing & \mathbf{G}_{j_-,k} \\ \varnothing & \mathbf{G}_{k,k} \end{bmatrix} \begin{Bmatrix} \mathbf{t}_i \\ \mathbf{t}_k \end{Bmatrix} \tag{29}$$

which, as in the previous case, must be understood as a part of the complete system if more regions or boundaries are present.

3.2.2 Cross-section stress resultants calculation

The solution at a point $\mathbf{x}^{\mathrm{i}}$ inside a domain Ω (internal point) is obtained in a post-processing stage by using the interior SBIE and its derivatives. The interior SBIE can

be directly applied to obtain displacement $\mathbf{u}^{\mathrm{i}}$, while an appropriate combination of its derivatives can be used to obtain strain $\varepsilon^{\mathrm{i}}_{lk}$ and stress σ^{i}_{lk} tensors. In particular, the so-called interior Hypersingular Boundary Integral Equation (HBIE) allows the calculation of traction $t^{\mathrm{i}}_l = \sigma^{\mathrm{i}}_{lk} n^{\mathrm{i}}_k$ at $\mathbf{x}^{\mathrm{i}}$ as:

$$t^{\mathrm{i}}_l = \int_{\partial\Omega} d^*_{lk} t_k \,\mathrm{d}\Gamma - \int_{\partial\Omega} s^*_{lk} u_k \,\mathrm{d}\Gamma, \quad l,k = 1,2,3 \tag{30}$$

where u_k and t_k are already known, and d^*_{lk} and s^*_{lk} are the hypersingular fundamental solutions which can be found elsewhere [see e.g. 33]. Numerical integration of this equation is particularly difficult because of the presence of quasi-singular integrals of order up to $\mathcal{O}\left(r^{-7}\right)$, where r is the distance between observation (any point $\mathbf{x} \in \partial\Omega$) point and collocation point $\mathbf{x}^{\mathrm{i}}$. An adaptive combination of cubic transformation and subdivision is used in this work [34, 35]. The interior HBIE can be used to determine stresses over pile virtual cross-sections, which after a proper integration leads to beam resultant forces and moments.

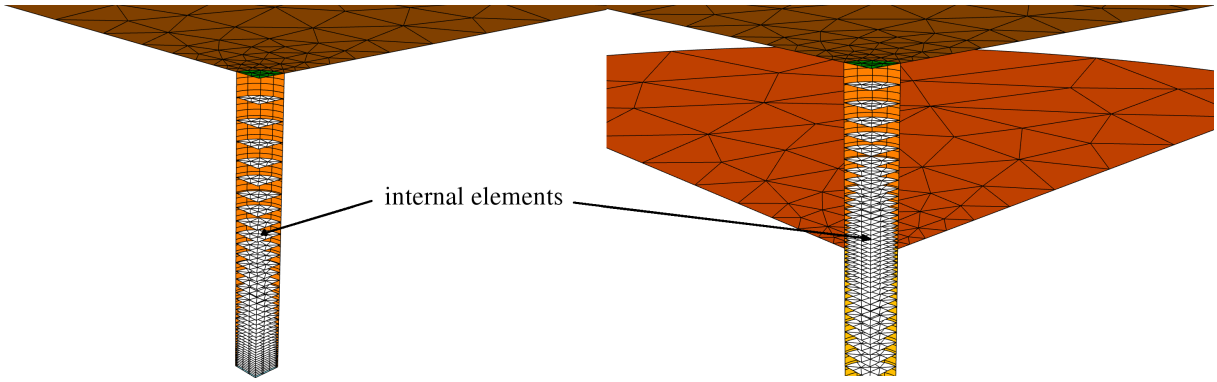

Figure 5: Pile cross-sections discretized into internal elements (white elements)

Each pile cross-section $\mathcal{X}$ is an oriented surface discretized into $N_{\mathcal{X}}$ elements (internal elements). Each internal element $\mathcal{E}$ of order R serves as a support for a set of internal points located at the integration points of a Gaussian quadrature of equal order. Let $N_{\mathcal{R}}$ be the number of integration points of the Gaussian quadrature, and $\boldsymbol{\eta}_j$ and w_j be the j-th quadrature point and weight, then global Cartesian forces and moments with respect to $\mathbf{x}_c$ are:

$$\mathbf{F}_{\mathcal{E}} = \int_{\mathcal{E}} \mathbf{t} \,\mathrm{d}S \approxeq \sum_{j=1}^{j=N_{\mathcal{R}}} \mathbf{t}^{\mathrm{i}}\left(\boldsymbol{\eta}_j\right) J\left(\boldsymbol{\eta}_j\right) w_j \tag{31a}$$

$$\mathbf{M}_{\mathcal{E}} = \int_{\mathcal{E}} (\mathbf{x} - \mathbf{x}_c) \times \mathbf{t} \,\mathrm{d}S \approxeq \sum_{j=1}^{j=N_{\mathcal{R}}} \left[\mathbf{x}\left(\boldsymbol{\eta}_j\right) - \mathbf{x}_c\right] \times \mathbf{t}^{\mathrm{i}}\left(\boldsymbol{\eta}_j\right) J\left(\boldsymbol{\eta}_j\right) w_j \tag{31b}$$

where J is the surface Jacobian. Finally, cross-section stress resultants are:

$$\mathbf{F}_{\mathcal{X}} = \sum_{\mathcal{X}} \mathbf{F}_{\mathcal{E}}, \quad \mathbf{M}_{\mathcal{X}} = \sum_{\mathcal{X}} \mathbf{M}_{\mathcal{E}} \tag{32}$$

Cross-sections are concentrated near the pile tip, and near the interface between strata, see Fig. 5. This is completely necessary in order to be able to capture the strong variations of shear force and bending moment near these pile locations.

4 Results and Discussion

In order to evaluate the influence of the tangential tractions on the estimation of pile maximum resultants for different scenarios, the properties of pile and soil shown in Table 2 are used. These properties are similar to the ones used for the seismic analysis of piles by other authors [36, 37].

Table 2: Pile and soil physical properties used in this study

Pile		Halfspace / Upper Layer		Bottom Layer (Rock)	
d (m)	0.6	c_s^1 (m/s)	110, 250, 350	c_s^2 (m/s)	800
L (m)	3, 6, 12, 24	$(E/E_s^1$	50, 100, 500)		
E (GPa)	30	ρ_s^1 (kg/m^3)	1750	ρ_s^2 (kg/m^3)	2500
ρ (kg/m^3)	2500	ν_s^1	0.4	ν_s^2	0.4
ν	0.25	β_s^1	5%	β_s^2	2%

Two soil profiles are considered: a homogeneous halfspace and a soil with two different layers. For the two-strata profile, the properties of the upper layer will coincide with the ones of the different studied halfspaces, while the bottom layer will present always the same properties (as indicated in Table 2). For this stratified profile, the interface between the two layers is assumed to be located at the half of the pile length ($h^1 = h^2 = L/2$).

As mentioned before, the work at hand also aims to study the performance of the BDWF model compared against a more rigorous continuous formulation (BEM). The description and assumptions of the different models used in the analyses are summarized in Table 3.

Regarding the computational demands of the BEM methodology, Table 4 shows the average time needed for solving each frequency and an approximation of the memory consumption for obtaining the results corresponding to the halfspace and two-layered profiles considering the medium-valued properties: $E/E_s = 100$ and $L = 12$ m. The low computational requirements of the BDWF model (less than 0.03s and 1MB in the worst

Table 3: Description of the models and contact conditions used in this study

Model	Description
B1	Continuous model. Smooth contact condition on the pile shaft. Free pile tip.
B3	Continuous model. Welded contact condition on the pile shaft. Free pile tip.
B4	Continuous model. Welded contact condition on the pile shaft and tip.
W1	Winkler model. Horizontal soil stiffness. Free pile tip.
W2	Winkler model. Horizontal and rocking soil stiffness. Free pile tip.
W3	Winkler model. Horizontal and rocking soil stiffness. m_I included. Free pile tip.
W4	Winkler model. Horizontal and rocking soil stiffness. m_I included. Loaded pile tip.
W*b	Winkler model assuming the Bernoulli's beam theory.

Table 4: Computational requirements of BEM model[1]: mean time per frequency and memory usage ($E/E_s = 100$ and $L = 12$ m)

Soil	Real time	CPU time	Memory
Halfspace	4.41 min	114.5 min	≈12.5 GB
Two-layers	8.56 min	221.9 min	≈25.7 GB

[1] run in a 28 cores (Intel® Xeon® CPU E5-2690 v4 @ 2.60GHz), 260 GB RAM computer

case scenario) makes it a suitable fast tool for the design stages; while the continuum model needs to be run in a high-performance computer. Attending to the times needed to compute each frequency, it is worth mentioning that the number of frequencies needed to obtain a suitable time response of the system through an Inverse Fast Fourier Transform algorithm should be carefully chosen when using the BEM model. The same procedure, but using all the required frequencies, can be completed by the Winkler model in a short amount of time.

4.1 Effects of the tangential tractions

The soil-pile interaction along the pile shaft is produced through the horizontal (t_x) and tangential (t_z) tractions acting between them. The firsts, produced by the contribution of the normal tractions (t_r) and the horizontal component of the tangential tractions (t_φ), see Fig. 2(b), are the ones of most importance. Nevertheless, the vertical tangential tractions (henceforth referred to just as tangential tractions), can also have an important role in the seismic response of the pile.

The soil-pile horizontal tractions are modelled in the BDWF formulation through the soil lateral stiffness K_x. These tractions, proportional to the horizontal relative displacement between pile and soil, constitute the main excitation of the beam. Thus, this component has to be always included into any Winkler model for the analysis of pile foundations.

On the other hand, the effects of the tangential stresses are usually not considered in BDWF models, or only the distributed moment produced by the rotation of the cross-section is included, see Fig. 2(c). However, this component does not represent the whole tangential tractions that participate in the problem of vertically incident S-waves. The effects of the tangential stresses originated by the distortion of the incident field can only be captured if the distributed moment produced (m_I) by its action is considered.

In order to illustrate the influence of the tangential tractions on the maximum resultants of the pile, Fig. 6 shows the envelopes of shear forces and bending moments obtained by different models. The results obtained through the BEM formulation are used as reference values. In this model, the tangential stresses on the soil-pile lateral interface are omitted or included by imposing smooth (B1) or welded (B3) boundary conditions, respectively. On the other hand, three BDWF models are considered: one does not include any tangential tractions by setting $K_\theta = K_I = 0$ (W1); while the others include the distributed moment of the tangential tractions produced only by the pile cross-section rotation, i.e. $K_I = 0$, (W2); or by both the pile rotation and by the action of the incident field (W3). For all models, free tip boundary conditions are assumed.

Attending to the obtained envelopes, the inclusion of the tangential tractions strongly

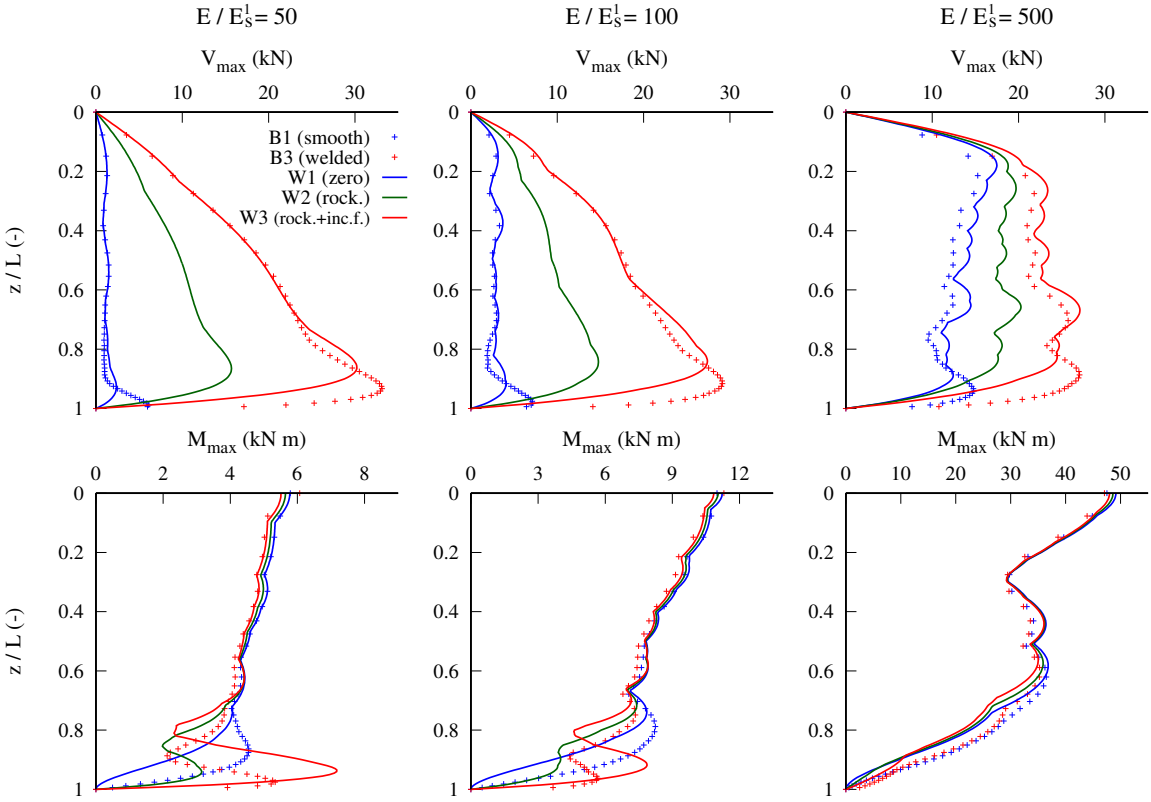

Figure 6: Analysis of the influence of the tangential tractions on the pile envelopes of maximum resultants. Pile length L=12 m (L/d=20). Halfspace profiles

alters the maximum shear forces of the pile: increasing their values along the whole beam. This increment is more important for harder soils. Related to this effect, the differences between the envelopes of shear forces for the three studied soils are reduced for the welded contact hypothesis, being the magnitude of their maximum value independent of the soil stiffness. This situation does not happen for the smooth contact condition. Regarding the distribution of maximum shear forces along the beam: for hard and moderately-hard soils ($E/E_s^1 = 50, 100$) including the effects of the tangential tractions makes the envelopes continuously increase with depth reaching the maximum value near pile tip; while for smooth conditions, the maximum shear forces remain with similar values for $z/L > 0.1$. On the contrary, for soft soils ($E/E_s^1 = 500$), the same trend is observed regardless the contact condition: no significant variations depending on the depth are found in the envelopes of shear forces for $z/L > 0.2$.

Regarding the ability of the proposed BDWF to reproduce the BEM envelopes, a good agreement is observed between the models with smooth contact conditions (W1 and B1). On the other hand, the obtained results also confirm that the soil rocking stiffness can not completely capture the effects of the tangential tractions acting over the pile. The envelopes obtained through this model (W2) are halfway from the ones corresponding to the model without any tangential tractions (W1) and the one that includes all of them (W3). For this reason, it can be concluded that both the rotation of the pile cross-section and the distortion of the incident field produce roughly the same tangential

tractions at the soil-pile interface (see Section 4.3). By including the rocking soil stiffness and the distributed moment produced by the incident field into the BDWF model, the envelopes of maximum shear forces of BEM formulation with welded boundary conditions can accurately be reproduced.

For envelopes of maximum bending moments of the pile, the inclusion of the tangential tractions is found to have little influence. All studied models yield virtually the same results. Only for the hardest soils at the pile tip, some differences can be appreciated depending on the contact conditions. For these hard soils, a high oscillation is produced near the pile tip when the tangential tractions are included for both the BDWF and BEM models. However, the peak that arises for the Winkler (W3) exceeds the values obtained by the continuous formulation. This behaviour is produced due to the exponential nature of the homogeneous solution, whose amplitudes are determined by the boundary conditions. The expressions of the beam bending moment and shear force include derivatives of several orders. Thus, nullifying their value at pile tip produces this highly oscillatory behaviour that vanishes as one moves away from the tip. In order to deepen this issue, the effects of assuming different boundary conditions are discussed in the next section.

4.2 Effects of the pile tip boundary conditions

The definition of the boundary conditions at the pile head and tip has a strong impact on its response at points near these ends, and can even modify the distribution of bending moments and shear forces along the whole beam.

The head boundary conditions are generally known with great accuracy because they are imposed by the union between the pile and the supported structure. For the incident S-wave problem, usually no lateral loads acting on the pile head are assumed so its horizontal displacement is considered free; while the rotation of the pile head can be assumed either as free (hinged union or free pile) or fixed (restrained by the supported structure). The fixed assumption is made in the present work because of the importance of adequately estimating the magnitude of the bending moment at pile head for this configuration.

On the contrary, boundary conditions at pile tip present higher uncertainties. For configurations where the pile tip reaches a perfectly rigid strata, it can be assumed that pile displacements at this end coincide with the ones of the bedrock and that the pile rotation is not allowed. This rotation restraint can be relaxed into a hinged condition assuming that the pile end plastifies due to the excessive loads acting over it. However, for configurations of piles embedded in a halfspace domain, where the beam end does not reach any rigid soil, the tip boundary conditions are not clearly determined. One general assumption is to consider a free tip, as has been done in the previous section. Another option is to assume that soil-pile interaction forces exist at the pile tip surface, similar to the ones acting on the pile shaft. This condition can be easily imposed in continuous models by assuming welded contact conditions, but not for the simplified formulations.

One solution for the Winkler models is to use a set of impedance functions for the pile end relating the tip rotations and displacements with the soil reactions acting over it, in the same manner that the soil-pile interaction along the pile length is modelled. However, there is a high uncertainty about the values or expressions for these tip-stiffness; being necessary, in some cases, an ad hoc estimation of them. Another alternative proposed in this work is to consider that at pile tip the shear force of the beam is equal to the horizontal

force that the tangential stresses of the incident field produce. This assumption follows the same idea as the inclusion of the distributed moment produced by the tangential tractions of the incident field along the pile shaft.

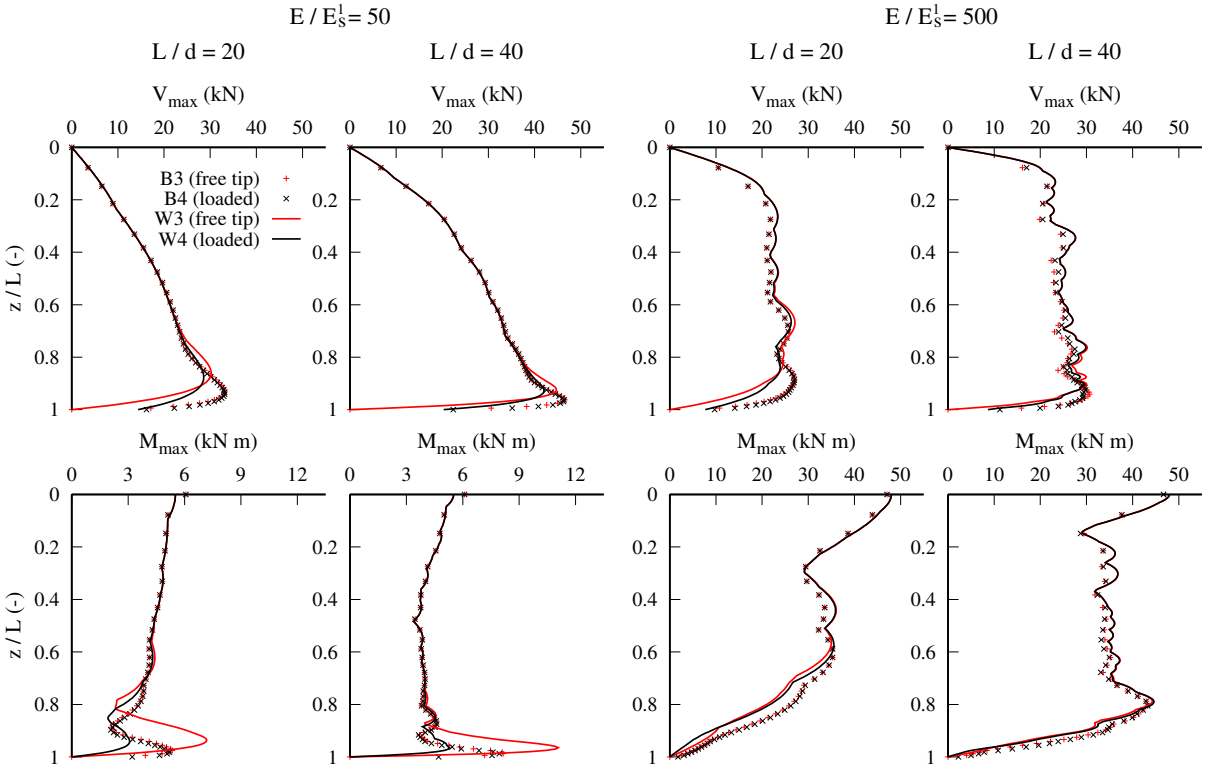

Figure 7: Analysis of the influence of the pile tip boundary conditions on the envelopes of maximum resultants. Pile lengths L=12 m (L/d=20) and L=24 m (L/d=40). Halfspace profiles

Fig. 7 shows the envelopes obtained by the formulations that include tangential tractions and assuming the two possibilities for the pile tip boundary conditions: free (B3 and W3) or loaded (B4 and W4). As mentioned before, the load condition is imposed by assuming welded boundary condition between the elements of the pile tip and the soil in the BEM formulation; and by including the shear force obtained from the incident field for the BDWF model. No results are shown for the models corresponding to smooth conditions as it would be not coherent to assume tangential interaction at pile tip but not along the pile shaft. The envelopes corresponding to different pile aspect ratios are presented in order to analyse the influence of the tip boundary conditions on the whole pile response.

For the continuous model, the changes in the boundary conditions only affect the value of the envelopes at pile tip, both for shear forces and bending moments. On the contrary, for the BDWF formulation these changes affects a longer portion of the pile end. The peak value of the envelopes of shear forces are slightly reduced by the new loaded boundary condition, while the pile tip force becomes non-zero (as expected) agreeing with the results obtained through the BEM. A different behaviour is found for the envelopes of maximum bending moments, which are affected to a greater extent by the changes of the

boundary conditions (especially for hard soils). Analysing the responses of the Winkler formulation, the results obtained by including the shear force produced by the incident field at the pile end present a better adjustment to the continuous solution. However, as the zero moment condition is kept, the Winkler model can not reproduce the bending moment values near the tip that are computed by the BEM.

These effects of the tip boundary conditions on the pile envelopes are found for all the pile aspect ratios. However, the portion of the pile that is affected by them is reduced for larger L/d ratios, as expected.

4.3 Results in terms of tangential tractions

This section aims to further illustrate the importance of each component of the tangential tractions and the ability of the BDWF formulation to reproduce their value along the pile shaft. Fig. 8 presents the real and imaginary part of the vertical tangential tractions that are obtained along the pile length for three different excitation frequencies. The results correspond to the line of maximum tangential tractions located at the points of the soil-pile interface whose coordinates are $x = d/2$ and $y = 0$. Three values of the excitation frequencies are selected in order to show the behaviour of the system in the low-, mid- and high-frequency ranges of interest.

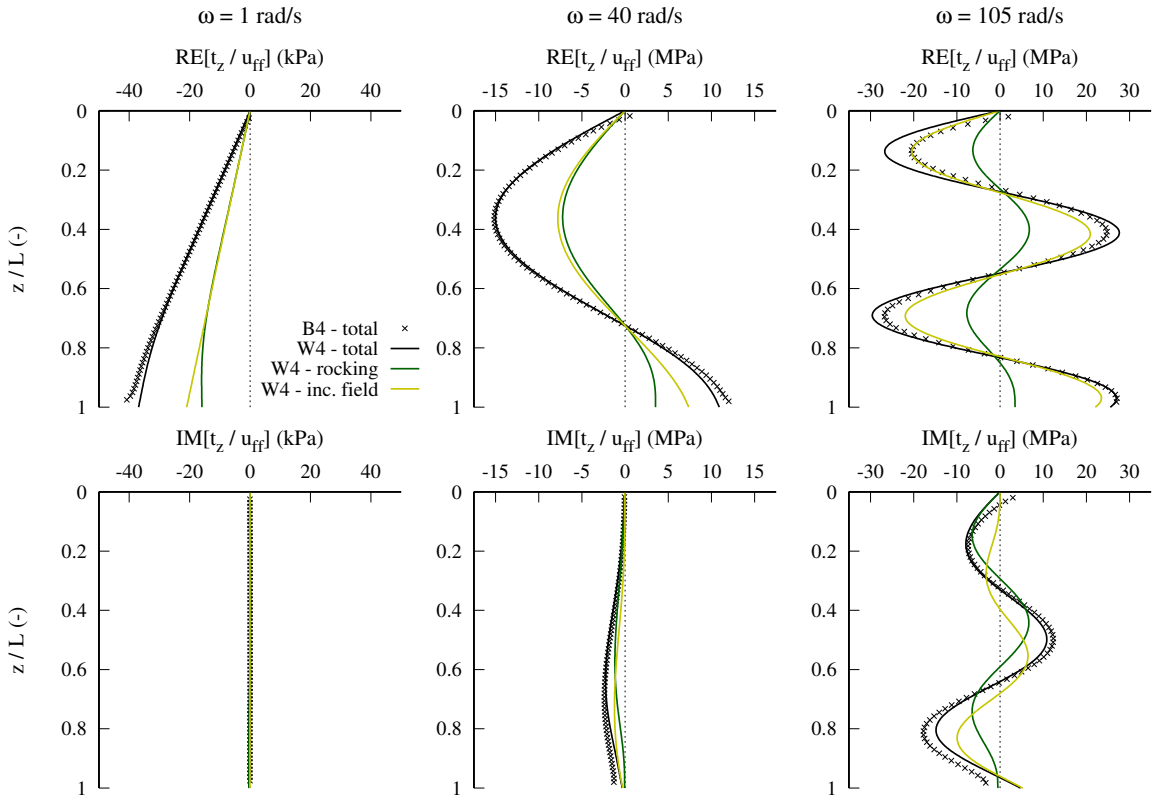

Figure 8: Maximum tangential tractions along the pile for various excitation frequencies. Pile length L=12 m (L/d=20). Halfspace profile E/E_s=500 (soft soil)

The total values of the tangential tractions computed by the Winkler model agree

very well with the results obtained by the continuous formulation. The highest differences between them are produced for the high-frequency range.

Fig. 8 confirms the fact that the tangential tractions that arise from the action of the incident field have the same importance as the ones produced by the pile rotation. The relevance of the former is even increased for the high-frequency response.

Regarding the values of the tangential tractions at pile tip, the results obtained by the BEM formulation can be adequately reproduced if the loaded tip conditions are assumed for the Winkler model.

4.4 Effects of the pile aspect ratio

Despite only slender beams have been considered in the previous analyses, pile foundations present a wide range of aspect ratios depending on their application or soil properties. For this reason, this section aims to study the influence of the pile aspect ratio on the obtained results.

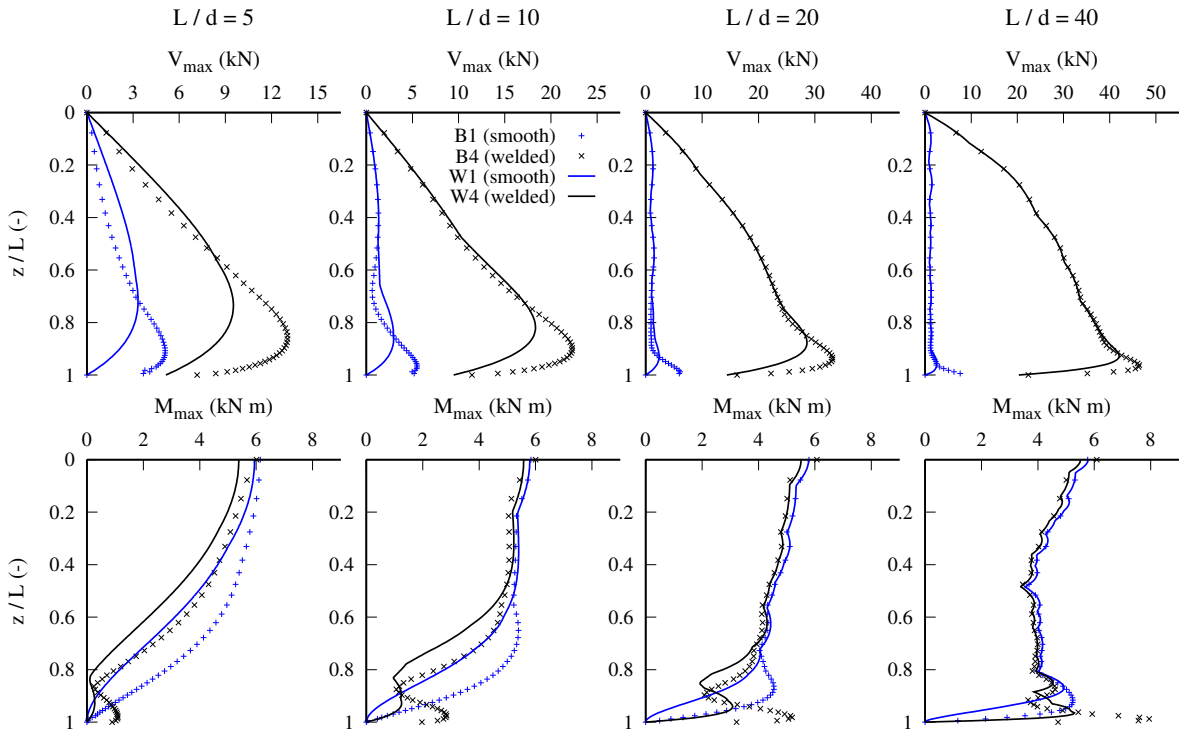

Figure 9: Analysis of the influence of the pile aspect ratio on the envelopes of maximum resultants. Halfspace profile E/E_s=50 (hard soil)

Fig. 9 shows the envelopes computed through the BEM and BDWF models and considering the two studied contact conditions (smooth with free tip, and welded with loaded tip) for several pile aspect ratios and assuming a hard soil. The effects of the inclusion of the tangential tractions commented in the previous sections are produced for all the aspect ratios. In addition, if the tangential tractions are included, significantly higher values of the maximum shear forces are obtained as the pile becomes more slender.

On the other hand, the envelopes of bending moments along the shortest pile are slightly modified depending on the assumed contact condition, while for the slender piles these differences in the maximum bending moments can only be found for the lower portion of the pile.

Results from Fig. 9 also show that the Winkler models can not perfectly emulate the envelopes of maximum resultants in the case of short piles. This can be explained as the effects of the pile tip have influence on a larger portion of the pile length than for slender piles. The discrepancies obtained at the pile tip between the Winkler and the continuous model are produced due to the diffractions at the surroundings of the pile end that the BDWF formulation is not able to reproduce.

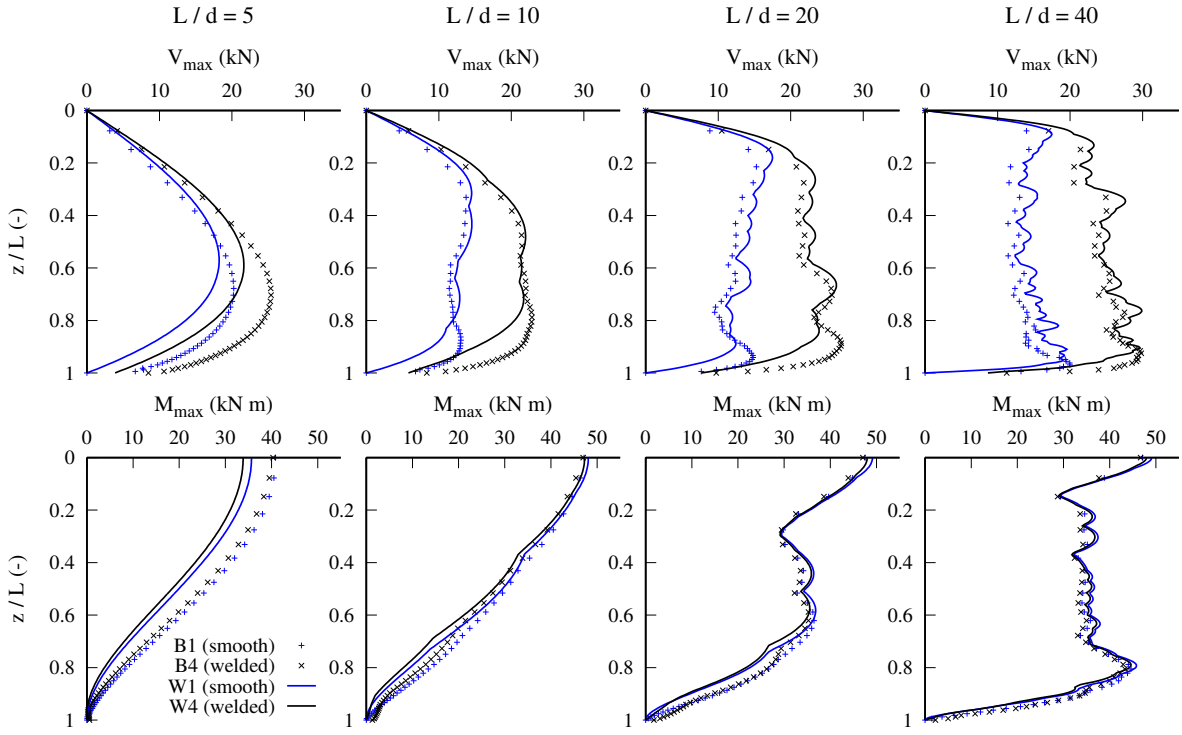

Figure 10: Analysis of the influence of the pile aspect ratio on the envelopes of maximum resultants. Halfspace profile E/E_s=500 (soft soil)

Fig. 10 now shows the envelopes for the configurations presented in Fig. 9 but for a softer soil. For this soil stiffness the discrepancies between the Winkler and continuous model are reduced, but still appreciable differences are found for short pile aspect ratios. Contrary to what happened for the hard profile, the pile slenderness has no significant influence on the magnitude of the maximum shear forces regardless of the contact condition for the soft soil.

4.5 Effects of the soil stratification

In the previous sections, the seismic response of a pile embedded in a homogeneous soil has been studied. However, it is also relevant to analyse the influence of the inclusion of

the tangential tractions and the ability of the BDWF model to estimate the pile envelopes in terrains with different layers. The study of these soil profiles is of vital importance, as great maximum resultants (especially bending moments) are produced at the depth where the soil properties abruptly change [36, 38–40].

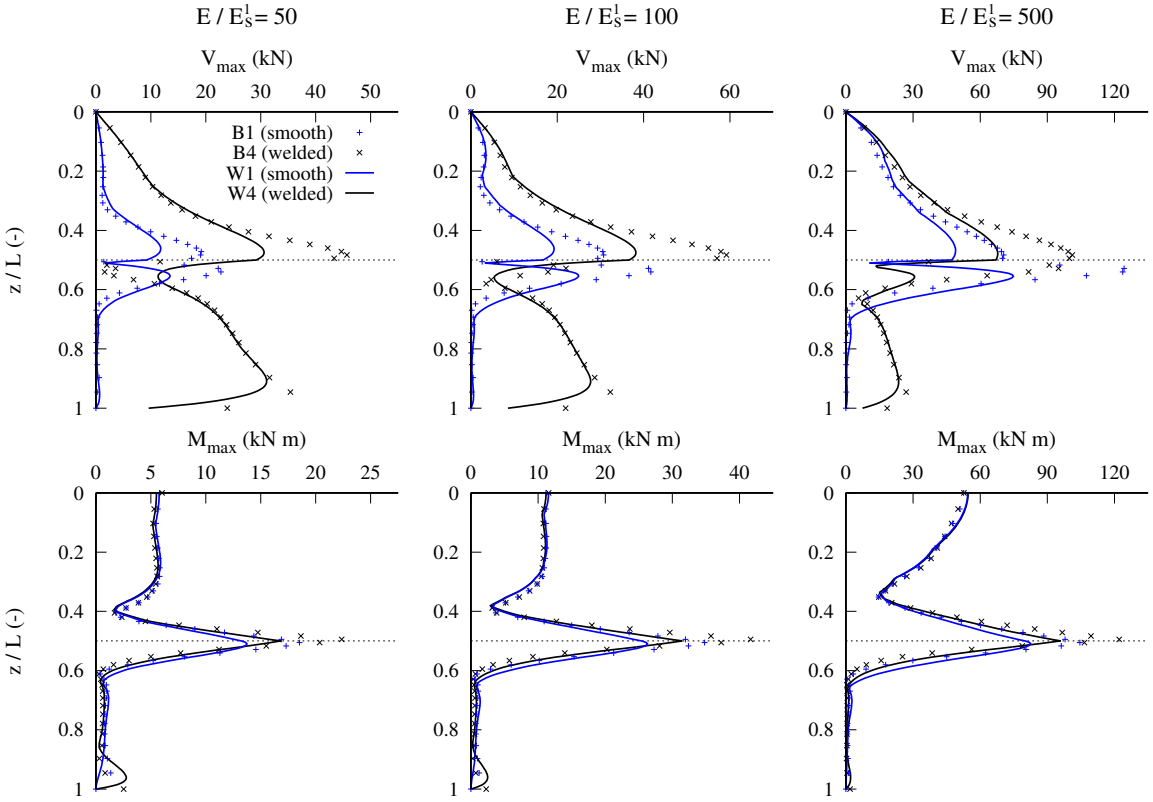

Figure 11: Analysis of the influence of the soil stratification on the pile envelopes of maximum resultants. Pile length L=12 m (L/d=20). Two-layered profiles

Fig. 11 shows the envelopes for three soils profiles with two different layers, whose properties of the upper layer change. Results obtained through the BEM and BDWF formulations are displayed both including and omitting the effects of the tangential tractions. As in the previous section, for the cases where they are included, the loaded tip boundary condition is assumed.

The effects of the contact conditions already commented in Section 4.1 are also observed for the stratified profiles: important increments in the maximum shear forces, especially for hard soils; while bending moments are affected to a minor extent. For the two-layered profiles, for which the maximum bending moments are located at the layer interface, the inclusion of the tangential tractions augments its value. In contrast, the envelope of bending moments along the rest of the pile is almost unaffected by the assumed contact condition.

On the other hand, two important variations in the distribution of maximum shear forces are found if the tangential tractions are included. First, at the interface surroundings, the peaks of the shear envelopes take place in the softer layer instead of in the rock

layer. And second, the shear forces along the pile shaft embedded in the rock stratum are strongly increased. The latter effect is expected as the influence of the tangential tractions is greater for harder soils.

The Winkler models reproduce the envelopes of their corresponding continuous models. However, the magnitude of the maximum resultants computed by the simplified formulation underestimates the values obtained from the BEM, both for the shear forces and bending moments. Those differences become more important around the layer interface, where the highest values of the envelopes take place.

4.6 Effects of the beam theory used in the BDWF model

In this study, the Timoshenko's beam theory has been used for modelling the pile because of its generality and accuracy. However, as piles are usually long, slender structures, they can be represented through the Bernoulli's beam theory. The use of this theory in the proposed BDWF formulation yields simpler and more compact expressions, which are detailed in B. The current section aims to compare the results obtained through the two different beam theories in order to discern under which assumptions the simpler formulation is enough to represent the pile seismic behaviour. Note that, because of the fact that the Bernoulli's theory is a common hypothesis in published models for pile foundations, this analysis is relevant for the interested reader.

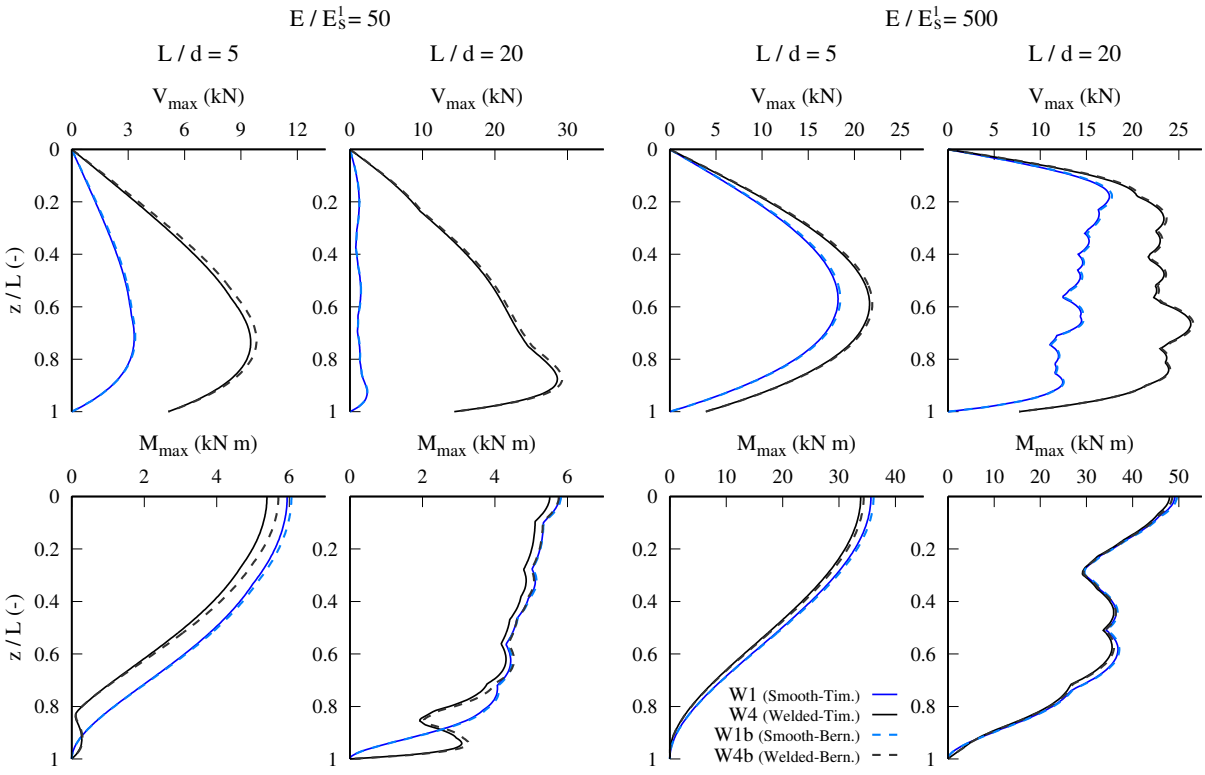

Figure 12: Analysis of the influence of the pile beam theory on the envelopes of maximum resultants. Pile lengths L=3 m (L/d=5) and L=12 m (L/d=20). Halfspace profiles

The envelopes obtained through the BDWF models both including or not the tangen-

tial tractions and using the Timoshenko's and Bernoulli's beam theories are presented in Fig. 12 for the soft and hard halfspaces. Two pile aspect ratios are analysed as greater differences between the Timoshenko's and Bernoulli's piles are expected for lower slenderness ratio. The obtained results confirm this hypothesis. However, for the models with smooth boundary conditions, the results of the different theories are found to be marginal; while some differences can be observed if the tangential tractions effects are considered, even for very slender piles. For these high pile aspect ratios, the bending moments obtained by using the Bernoulli assumptions are insensitive to the inclusion of the tangential tractions for the upper half of the pile ($z/L < 0.6$).

Regarding the effect of the soil stiffness, the discrepancies between the two beam theories are further reduced for soft profiles independently of the soil-pile contact condition. For all the studied configurations, the Bernoulli assumption is a conservative one as it yields slightly higher shear and moment resultants than the Timoshenko's theory.

5 Conclusions

In this work, the influence of the tangential tractions on the seismic maximum bending moments and shear forces of a pile embedded in a homogeneous halfspace and a bi-strata domain has been evaluated through a Winkler formulation. Also, the use of the proposed BDWF model for the estimation of the pile seismic response has been tested by comparing its performance with respect to a more rigorous model of the continuum solid based on BEM. The principal conclusions drawn from the obtained results are:

- The tangential tractions have a strong impact on the pile maximum shear forces, significantly increasing their values. On the contrary, the maximum bending moments of the pile are virtually unaffected by the pile-soil contact conditions. The effects of the tangential tractions are more important for hard soils.

- In order to reproduce the welded contact condition with the Winkler formulation, both the distributed moments produced by the rotation of the pile cross-section and by the action of the incident field have to be included.

- The BDWF model can be used to accurately estimate the envelopes of slender piles embedded in homogeneous soils. However, for shorter piles, some differences arise between the results of the simplified and continuous formulations.

- The use of the proposed Winkler formulation for the analysis of piles in soils that present layers with different properties may underestimate the high moments and forces that are produced at the layer interface when compared to the BEM results.

- The use of the Bernoulli's theory for modelling the piles in this problem is an acceptable option, as practically no differences are found with respect to the Timoshenko's beam theory. Furthermore, in case some discrepancies arise, the Bernoulli assumption is a conservative one.

A Derivation of the equations for the Timoshenko's beam Winkler model

In this Appendix, the detailed procedure followed in order to obtain Eqs. from (15) to (22) is presented. For simplicity's sake, the super-index related to the soil layer is omitted and the variables are expressed as functions of the dimensionless axial coordinate $\xi = z/h$. Note that $\mathrm{d}/\mathrm{d}z = (1/h)\ \mathrm{d}/\mathrm{d}\xi$.

A.1 Rotation of beam section θ (Eq. 20)

In order to obtain the differential equation in terms of the lateral displacements of the beam, u, first the expression of the section rotation θ in terms of u has to be obtained from Eq. (12):

$$\theta = \frac{EI}{\alpha GA}\left[\frac{1}{(h)^3}\frac{\mathrm{d}^3u}{\mathrm{d}\xi^3} + \frac{\alpha GA}{EI}\frac{1}{h}\frac{\mathrm{d}u}{\mathrm{d}\xi} + \frac{1}{\alpha GA}\frac{1}{h}\frac{\mathrm{d}q}{\mathrm{d}\xi} + \frac{1}{EI}m\right] \tag{33}$$

Including the expressions of the distributed load (13) and moments (14):

$$\theta = \frac{EI}{\alpha GA}\left[\frac{1}{(h)^3}\frac{\mathrm{d}^3u}{\mathrm{d}\xi^3} + \frac{\alpha GA}{EI}\frac{1}{h}\frac{\mathrm{d}u}{\mathrm{d}\xi} + \frac{\left(\rho A\omega^2 - K_x\right)\frac{\mathrm{d}u}{\mathrm{d}\xi} + K_x\frac{\mathrm{d}u_I}{\mathrm{d}\xi}}{\alpha GA\ h} + \frac{\left(\rho I\omega^2 - K_\theta\right)\theta - K_I\frac{1}{h}\frac{\mathrm{d}u_I}{\mathrm{d}\xi}}{EI}\right] \tag{34}$$

Rearranging the terms in order to obtain the dimensionless coefficients from Table 1, and separating the rotation of the beam section:

$$\begin{aligned}\theta =& \frac{EI(1/h)}{\alpha GA\ (h)^2}\left[\frac{\mathrm{d}^3u}{\mathrm{d}\xi^3} + \left(\frac{\alpha GA(h)^2}{EI} + \frac{\left(\rho A\omega^2 - K_x\right)(h)^2}{\alpha GA}\right)\frac{\mathrm{d}u}{\mathrm{d}\xi} + \left(\frac{K_x(h)^2}{\alpha GA} - \frac{K_I(h)^2}{EI}\right)\frac{\mathrm{d}u_I}{\mathrm{d}\xi}\right] \\ &+ \frac{\left(\rho I\omega^2 - K_\theta\right)}{\alpha GA}\theta\end{aligned} \tag{35}$$

Grouping the pile rotation terms and solving, the expression of the pile rotation in terms of the lateral displacements is finally obtained as:

$$\begin{aligned}\theta =& \frac{(1/h)}{\left(\frac{\alpha GA}{EI} - \frac{\rho I\omega^2 - K_\theta}{EI}\right)\ (h)^2}\left[\frac{\mathrm{d}^3u}{\mathrm{d}\xi^3} + (\kappa_3 - \kappa_1)\frac{\mathrm{d}u}{\mathrm{d}\xi} + (\kappa_4 - \kappa_5)\frac{\mathrm{d}u_I}{\mathrm{d}\xi}\right] \\ =& \frac{(1/h)}{\kappa_3 + \kappa_2}\left[\frac{\mathrm{d}^3u}{\mathrm{d}\xi^3} - (\kappa_1 - \kappa_3)\frac{\mathrm{d}u}{\mathrm{d}\xi} + (\kappa_4 - \kappa_5)\frac{\mathrm{d}u_I}{\mathrm{d}\xi}\right]\end{aligned} \tag{36}$$

A.2 Bending moment M and shear force V (Eqs. 21,22)

Once the expression of the beam rotation in terms of the lateral displacements is known, the one of the bending moment can be simply obtained by substituting the expression of θ (36) into Eq. (10a) as:

$$M = EI\frac{1}{h}\frac{\mathrm{d}\theta}{\mathrm{d}\xi} = \frac{EI/(h)^2}{\kappa_3 + \kappa_2}\left[\frac{\mathrm{d}^4u}{\mathrm{d}\xi^4} - (\kappa_1 - \kappa_3)\frac{\mathrm{d}^2u}{\mathrm{d}\xi^2} + (\kappa_4 - \kappa_5)\frac{\mathrm{d}^2u_I}{\mathrm{d}\xi^2}\right] \tag{37}$$

While the expression of the shear force is obtained by substituting the expression of θ (36) into Eq. (10b) and grouping the terms corresponding to $\mathrm{d}u/\mathrm{d}\xi$:

$$V = \alpha GA\left(\frac{1}{h}\frac{\mathrm{d}u}{\mathrm{d}\xi} - \theta\right) = \frac{(\alpha GA/h)}{\kappa_3+\kappa_2}\left[\frac{\mathrm{d}^3u}{\mathrm{d}\xi^3} + (\kappa_1+\kappa_2)\frac{\mathrm{d}u}{\mathrm{d}\xi} + (\kappa_4-\kappa_5)\frac{\mathrm{d}u_I}{\mathrm{d}\xi}\right] \tag{38}$$

A.3 BDWF differential governing equation (Eq. 15)

Now, from the general expression of the differential equation (11):

$$\frac{1}{(h)^4}\frac{\mathrm{d}^4u}{\mathrm{d}\xi^4} + \frac{1}{\alpha GA}\frac{1}{(h)^2}\frac{\mathrm{d}^2q}{\mathrm{d}\xi^2} - \frac{q}{EI} + \frac{1}{EI}\frac{1}{h}\frac{\mathrm{d}m}{\mathrm{d}\xi} = 0 \tag{39}$$

Including the expressions of the distributed load (13) and moments (14) and using the dimensionless parameters (Table 1):

$$\frac{\mathrm{d}^4u}{\mathrm{d}\xi^4} - \kappa_1\frac{\mathrm{d}^2u}{\mathrm{d}\xi^2} + \kappa_4\frac{\mathrm{d}^2u_I}{\mathrm{d}\xi^2} + (\kappa_1 u - \kappa_4 u_I)\,\kappa_3 - h\;\kappa_2\frac{\mathrm{d}\theta}{\mathrm{d}\xi} - \kappa_5\frac{\mathrm{d}^2u_I}{\mathrm{d}\xi^2} = 0 \tag{40}$$

Substituting the derivative of the pile rotation (36):

$$\begin{aligned}\frac{\mathrm{d}^4u}{\mathrm{d}\xi^4} - \kappa_1\frac{\mathrm{d}^2u}{\mathrm{d}\xi^2} + \kappa_4\frac{\mathrm{d}^2u_I}{\mathrm{d}\xi^2} + (\kappa_1 u - \kappa_4 u_I)\,\kappa_3 \\ - \frac{\kappa_2}{\kappa_2+\kappa_3}\left[\frac{\mathrm{d}^4u}{\mathrm{d}\xi^4} - (\kappa_1-\kappa_3)\frac{\mathrm{d}^2u}{\mathrm{d}\xi^2} + (\kappa_4-\kappa_5)\frac{\mathrm{d}^2u_I}{\mathrm{d}\xi^2}\right] - \kappa_5\frac{\mathrm{d}^2u_I}{\mathrm{d}\xi^2} = 0\end{aligned} \tag{41}$$

Grouping together the terms of each derivative, operating in order to have $\mathrm{d}^4u/\mathrm{d}\xi^4$ multiplied by one, and separating the displacements of the beam to the ones of the incident field, the governing equation is obtained as:

$$\frac{\mathrm{d}^4u}{\mathrm{d}\xi^4} - (\kappa_1+\kappa_2)\frac{\mathrm{d}^2u}{\mathrm{d}\xi^2} + \kappa_1(\kappa_2+\kappa_3)\,u = \kappa_4(\kappa_2+\kappa_3)\,u_I - (\kappa_4-\kappa_5)\frac{\mathrm{d}^2u_I}{\mathrm{d}\xi^2} \tag{42}$$

B Winkler model for an embedded Bernoulli's Beam

The choice of the Bernoulli's theory does not affect the equilibrium equations (9) obtained in Section 3.1, but the constitutive laws of the beam. With this beam theory, one has:

$$\theta = \frac{\mathrm{d}u}{\mathrm{d}z} \tag{43a}$$

$$M = EI\frac{\mathrm{d}\theta}{\mathrm{d}z} = EI\frac{\mathrm{d}^2u}{\mathrm{d}z^2} \tag{43b}$$

Substituting the new constitutive equations (43) in the equilibrium equations (9), the general differential equation for a Bernoulli beam subjected to a distributed load and moment results in:

$$\frac{\mathrm{d}^4u}{\mathrm{d}z^4} - \frac{q}{EI} + \frac{1}{EI}\frac{\mathrm{d}m}{\mathrm{d}z} = 0 \tag{44}$$

Note that the only difference between Eqs. (11) and (44) is the $\mathrm{d}^2q/\mathrm{d}z^2$ term. In addition, the expression of the shear force results in:

$$V = -EI\frac{\mathrm{d}^3u}{\mathrm{d}z^3} - m \tag{45}$$

Including the equations of the distributed force (13) and moment (14) in the differential equation (44) and using the dimensionless axial variable ξ, the differential equation that governs the lateral displacements for this beam theory can be expressed in terms of the dimensionless coefficients of Table 1 as:

$$\frac{\mathrm{d}^4u}{\mathrm{d}\xi^4} - \kappa_2\frac{\mathrm{d}^2u}{\mathrm{d}\xi^2} + \kappa_1\kappa_3 u = \kappa_4\kappa_3 u_I + \kappa_5\frac{\mathrm{d}^2u_I}{\mathrm{d}\xi^2} \tag{46}$$

The solution of this equation is, again, the combination of the homogeneous and particular components. Expressions from (17) to (19) are still valid if the terms a_{1-4} are redefined as follow:

$$a_1 = \kappa_2 \tag{47a}$$
$$a_2 = \kappa_1\kappa_3 \tag{47b}$$
$$a_3 = \kappa_4\kappa_3 \tag{47c}$$
$$a_4 = -\kappa_5 \tag{47d}$$

As before, in order to obtain the amplitudes of the homogeneous part, the external (pile head and tip) and internal (at each layer interface) boundary conditions are applied. The expressions of the beam rotation, bending moment and shear force for this beam theory are:

$$\theta(\xi) = \frac{1}{h}\frac{\mathrm{d}u}{\mathrm{d}\xi} \tag{48}$$

$$M(\xi) = \frac{EI}{(h)^2}\frac{\mathrm{d}^2u}{\mathrm{d}\xi^2} \tag{49}$$

$$V(\xi) = \frac{-EI}{(h)^3}\left[\frac{\mathrm{d}^3u}{\mathrm{d}\xi^3} - \kappa_2\frac{\mathrm{d}u}{\mathrm{d}\xi} - \kappa_5\frac{\mathrm{d}u_I}{\mathrm{d}\xi}\right] \tag{50}$$

Acknowledgements

The authors would like to thank Prof. Luis A. Padrón for his constructive comments that undoubtedly improved the quality of the present work.

This work was supported by the Subdirección General de Proyectos de Investigación of the Ministerio de Economía y Competitividad (MINECO) of Spain and FEDER through research project BIA2014-57640-R.

G.M. Álamo (FPU14/06115) and J.D.R. Bordón (FPU13/01224) are recipients of FPU research fellowships from the Ministerio de Educación, Cultura y Deporte of Spain.

Gmsh has been used as mesh generator, pre- and post-processing utility [41] in this paper. The authors would like to appreciate the effort of this team in providing this software to the community.

References

[1] Mizuno, H.. Pile damage during earthquake in Japan (1923-1983). In: Nogami, T., editor. Dynamic Response of Pile Foundations - Experiment, Analysis and Observation. New York: Geotechnical Special Publication ASCE; 1987, p. 53–78.

[2] Tazoh, T., Shimizu, K., Wakahara, T.. Seismic observations and analysis of grouped piles. In: Nogami, T., editor. Dynamic Response of Pile Foundations - Experiment, Analysis and Observation. New York: Geotechnical Special Publication ASCE; 1987, p. 1–20.

[3] Nikolaou, S., Mylonakis, G., Gazetas, G., Tazoh, T.. Kinematic pile bending during earthquakes: analysis and field measurements. Geotechnique 2001;51(5):425–440.

[4] Hussien, M.N., Tobita, T., Iai, S., Karray, M.. Soil-pile-structure kinematic and inertial interaction observed in geotechnical centrifuge experiments. Soil Dyn Earthq Eng 2016;89:75–84.

[5] Froio, D., Rizzi, E.. Analytical solution for the elastic bending of beams lying on a variable winkler support. Acta Mech 2016;227(4):1157–1179.

[6] Çatal, S.. Solution of free vibration equations of beam on elastic soil by using differential transform method. Appl Math Model 2008;32:1744–1757.

[7] Miao, Y., Shi, Y., Luo, H., Gao, R.. Closed-form solution considering the tangential effect under harmonic line load for an infinite Euler-Bernoulli beam on elastic foundation. Appl Math Model 2018;54:21–33.

[8] Gazetas, G., Dobry, R.. Horizontal response of piles in layered soils. J Geotech Eng 1984;110(1):20–40.

[9] Yesilce, Y., Catal, H.H.. Free vibration of piles embedded in soil having different modulus of subgrade reaction. Appl Math Model 2008;32:889–900.

[10] Liang, F., Li, Y., Li, L., Wang, J.. Analytical solution for laterally loaded long piles based on Fourier-Laplace integral. Appl Math Model 2014;38:5198–5216.

[11] Flores-Berrones, R., Whitman, R.V.. Seismic response of end-bearing piles. J Geotech Eng Div 1982;108(4):554–569.

[12] Dobry, R., O'Rourke, M.J.. Discussion of 'Seismic Response Of End-bearing Piles' by R. Flores-Berrones and R. V. Whitman. J Geotech Eng 1983;109(5):778–781.

[13] Kavvadas, M., Gazetas, G.. Kinematic seismic response and bending of free-head piles in layered soil. Geotechnique 1993;43(2):207–222.

[14] Dezi, F., Carbonari, S., Leoni, G.. A model for the 3D kinematic interaction analysis of pile groups in layered soils. Earthq Eng Struct Dyn 2009;38:1281–1305.

[15] Anoyatis, G., Di Laora, R., Mandolini, A., Mylonakis, G.. Kinematic response of single piles for different boundary conditions: Analytical solutions and normalization schemes. Soil Dyn Earthq Eng 2013;44:183–195.

[16] Rovithis, E., Mylonakis, G., Pitilakis, K.. Dynamic stiffness and kinematic response of single piles in inhomogeneous soil. Bull Earthq Eng 2013;11:1949–1972.

[17] Kampitsis, A., Sapountzakis, E., Giannakos, S., Gerolymos, N.. Seismic soil-pile-structure kinematic and inertial interaction-A new beam approach. Soil Dyn Earthq Eng 2013;55:211 – 224.

[18] Gerolymos, N., Gazetas, G.. Winkler model for lateral response of rigid caisson foundations in linear soil. Soil Dyn Earthq Eng 2006;26(5):347–361.

[19] Chopra, A.K.. Dynamic of structures. Theory and applications to earthquake engineering. NJ: Prentice-Hall; 2001.

[20] Eurocode, . Eurocode 8: Design of structures for earthquake resistance. Part 5: Foundations, Retaining Structures and Geotechnical Aspects. European Committee for Standardization, Brussels. 2004.

[21] Novak, M., Nogami, T., Aboul-Ella, F.. Dynamic soil reaction for plane-strain case. J Eng Mech Div 1978;104(4):953–959.

[22] Roesset, J.M.. The use of simple models in soil-structure interaction. In: Second ASCE Conference on Civil Engineering and Nuclear Power. Knoxville; 1980,.

[23] Gazetas, G., Dobry, R.. Simple radiation damping model for piles and footings. J Eng Mech 1984;110(6):937–956.

[24] Mylonakis, G.. Simplified model for seismic pile bending at soil layer interfaces. Soils Found 2001;41(4):47–58.

[25] Domínguez, J.. Boundary Elements in Dynamics. International Series on Computational Engineering; Computational Mechanics Publications; 1993.

[26] Maeso, O., Aznárez, J.J., García, F.. Dynamic impedances of piles and groups of piles in saturated soils. Comput Struct 2005;83:769–782.

[27] Bordón, J.D.R., Aznárez, J.J., Maeso, O.. Dynamic model of open shell structures buried in poroelastic soils. Comput Mech 2017;60(2):269–288.

[28] Medina, C., Padrón, L.A., Aznárez, J.J., Santana, A., Maeso, O.. Kinematic interaction factors of deep foundations with inclined piles. Earthq Eng Struct Dyn 2014;43(13):2035–2050.

[29] Beer, G., Smith, I., Duenser, C.. The Boundary Element Method with Programming. Springer Wien New York; 2008.

[30] Li, H.B., Han, G.M., Mang, H.A.. A new method for evaluating singular integrals in stress analysis of solids by the direct boundary element method. Int J Numer Meth Eng 1985;33:2071–2098.

[31] Chirino, F., Maeso, O., Aznárez, J.J.. Una técnica simple para el cálculo de las integrales en el sentido del valor principal en el MEC 3D. Rev Int Metod Numer 1998;16:77–95.

[32] Mantič, V.. A new formula for the C-matrix in the Somigliana identity. J Elasticity 1993;33:191–201.

[33] Domínguez, J., Ariza, M.P., Gallego, R.. Flux and traction boundary elements without hypersingular or strongly singular integrals. Int J Numer Methods Eng 2000;48:111–135.

[34] Jun, L., Beer, G., Meek, J.. Efficient evaluation of integrals of order $1/r$, $1/r^2$ and $1/r^3$ using Gauss quadrature. Eng Anal 1985;2(3):118–123.

[35] Telles, J.. A self-adaptive co-ordinate transformation for efficient numerical evaluation of general boundary element integrals. Int J Numer Methods Eng 1987;24:959–973.

[36] Dezi, F., Carbonari, S., Leoni, G.. Kinematic bending moments in pile foundations. Soil Dyn Earthq Eng 2010;30(3):119–132.

[37] Padrón, L.A., Suárez, A., Aznárez, J.J., Maeso, O.. Kinematic internal forces in deep foundations with inclined piles. Earthq Eng Struct Dyn 2015;44(12):2129–2135.

[38] de Sanctis, L., Maiorano, R.M.S., Aversa, S.. A method for assessing kinematic bending moments at the pile head. Earthq Eng Struct Dyn 2010;39:1133–1154.

[39] Sica, S., Mylonakis, G., Simonelli, A.L.. Strain effects on kinematic pile bending in layered soil. Soil Dyn Earthq Eng 2013;49:231–242.

[40] Martinelli, M., Burghignoli, A., Callisto, L.. Dynamic response of a pile embedded into a layered soil. Soil Dyn Earthq Eng 2016;87:16–28.

[41] Geuzaine, C., Remacle, J.F.. Gmsh: a three-dimensional finite element mesh generator with built-in pre- and post-processing facilities. Int J Numer Methods Eng 2009;79(11):1309–1331.